

DESIGN OPTIMIZATION OF A FULLY-COMPLIANT BISTABLE MICRO-MECHANISM

Brian D. Jensen

Department of Mechanical
Engineering
University of Michigan
Ann Arbor MI 48109-2125
bdjensen@umich.edu

Matthew B. Parkinson

Biomedical Engineering Department
University of Michigan
Ann Arbor MI 48109-2125
mparkins@umich.edu

Katsuo Kurabayashi

Department of Mechanical
Engineering
University of Michigan
Ann Arbor MI 48109-2125
katsuo@umich.edu

Larry L. Howell

Mechanical Engineering Department
Brigham Young University
Provo UT 84602
lhowell@et.byu.edu

Michael S. Baker

MEMS Device Technologies
Sandia National Laboratories
Albuquerque NM 87185
msbaker@sandia.gov

ABSTRACT

Bistable behavior is desirable for a variety of applications because power is applied only during switching, and the mechanism state remains the same regardless of any power interruptions. The low variability in the stable positions also makes accurate open-loop control of many systems possible, and the precise switching characteristics make them valuable in sensing arrays. In this paper, fully-compliant bistable micromechanisms were modeled using finite elements. This model was then coupled with an optimization program, allowing extensive exploration of the design space. Three designs within this space were generated by minimizing the layout size of the devices subject to force constraints. These designs were subsequently manufactured and tested to verify bistability, with each mechanism snapping as expected between the two stable positions. The design space was then further explored to determine the behavior of the device as the maximum force output increased. This study revealed that the minimum layout size increases with the maximum force output.

INTRODUCTION

Bistable micromechanisms remain in stable equilibrium in two distinct positions. This behavior is valuable for several

MEMS applications because power is applied only to switch the mechanism, and the state of the mechanism is not lost upon interruption of power to the system. Furthermore, the low variability in their stable positions makes accurate open-loop control of many systems possible. For example, mechanically bistable devices have been investigated for use as microvalves [1-4], nonvolatile memory elements [5], micro-switches or relays [6-11], and fiber-optic switches [12-14]. The possibility of open-loop control has also led to work on a bistable display system [15]. Moreover, the precise switching capabilities of bistable devices has also made them attractive as sensing arrays [16].

Many of these reported devices rely on residual stress to induce beam buckling, a well-known bistable phenomenon. However, the difficulty of accurately controlling residual stress in micromachined materials complicates reproducibility of such devices [17,18]. Recently, bistable devices which operate in the absence of residual stress, making them more reliable [11,19], have been proposed. This also allows fabrication using deep reactive ion etching of single-crystal silicon substrates or within foundry-type processing for technologies which minimize residual stress in mechanical materials. However, the design of these mechanisms is made difficult by the necessity to keep stress low to avoid fracture. Moreover, the design must be

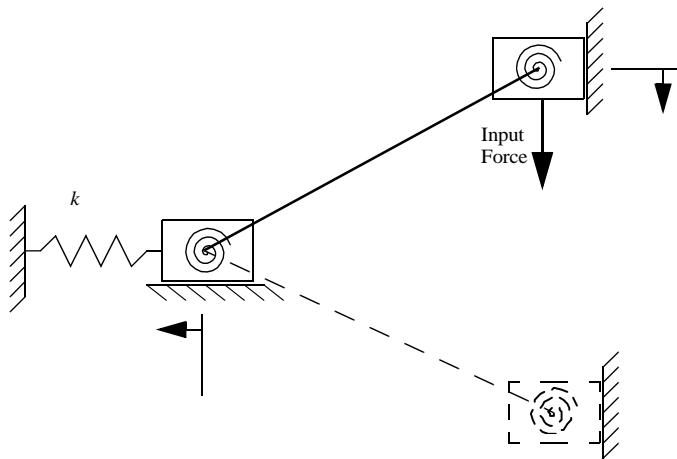


Figure 1: The rigid-body mechanism model

considered carefully to ensure that switching will occur, as many designs fail to toggle [11,19]. Finally, a fully-compliant, one-piece design is desirable to avoid friction, backlash, and wear at joints [20,21].

This paper further explores the mechanism typology of [19] to demonstrate operation of fabricated fully-compliant bistable mechanisms. Also, the force-generation capabilities of the mechanism typology within one fabrication technology are explored. Specifically, mechanism designs are generated for the SUMMiT-V technology, Sandia National Laboratory's five-layer polysilicon surface micromachining technology. In order to explore the design space quickly, optimization techniques are used. Testing shows that the devices work as expected, and the data generated are used to understand better the nature of fully-compliant bistable micromechanism designs.

MECHANISM DESIGN

The mechanism typology is inspired by the rigid-body mechanism model shown in Fig. 1 [19]. This mechanism model incorporates two sliders joined by a rigid link. The slider at the left is attached to a relatively stiff spring, which pushes the mechanism into a second stable position as shown in dashed lines. A torsional spring acts at each pin joint to represent the fully-compliant mechanism's resistance to bending. These two torsional springs remain deflected in the second stable position, so that they work against the action of the side spring. Hence, if the spring stiffness k is not large enough for a given design, the torsional springs will prevent the mechanism from possessing a second stable position.

The rigid-body model of Fig. 1 may be converted to a fully-compliant micromechanism design using pseudo-rigid-body modeling, in which rigid-body joints are replaced by one or more flexible segments [21,22]. The illustration in Fig. 2 demonstrates the micromechanism typology for this case. Here, the top slider is approximated by mirroring the mechanism. Then, the torsional

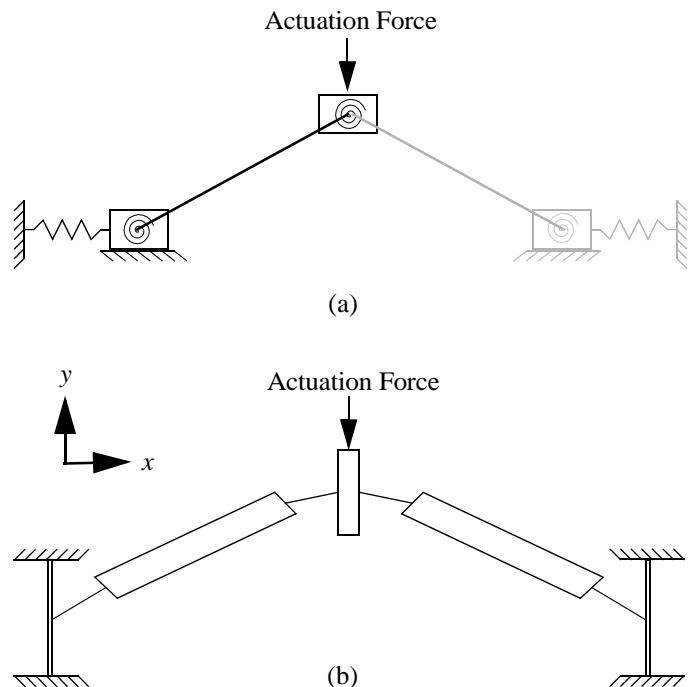


Figure 2: Conversion of rigid-body model to fully-compliant micromechanism

springs are replaced with thin flexible members and the side spring is replaced with a fixed-fixed beam. The fixed-fixed beam is much stiffer in the transverse direction than it is axially; so that it also approximates the motion of the other slider.

Finite Element Model

This mechanism typology tends to experience large-deflection behavior during deflection, complicating analytical modeling. Therefore, a nonlinear finite element model was created using beam elements in ANSYS. The model was parameterized to allow easy calculation of behavior for any conceivable device dimensions, with parameters illustrated in Fig. 3. The finite element model calculates the force required to move the mechanism to 32 points along its deflection path. Maximum stress in the device at each step is also recorded.

Fig. 4 shows a sample of the data resulting from the finite element model for a bistable mechanism design. This graph plots the displacement of the central translating element against the calculated force required to produce that displacement. The behavior is highly nonlinear, with the magnitude of the force initially rising to a maximum at the value denoted as F_{min} (because the initial sign of the force is negative, denoting a force in the $-y$ direction). Thereafter, the magnitude drops to zero at the unstable position. The mechanism will remain in this position in the absence of external forces, but any perturbations will cause it to "snap" into one of the two stable positions. Finally, the magnitude of force rises again, though in the other direction,

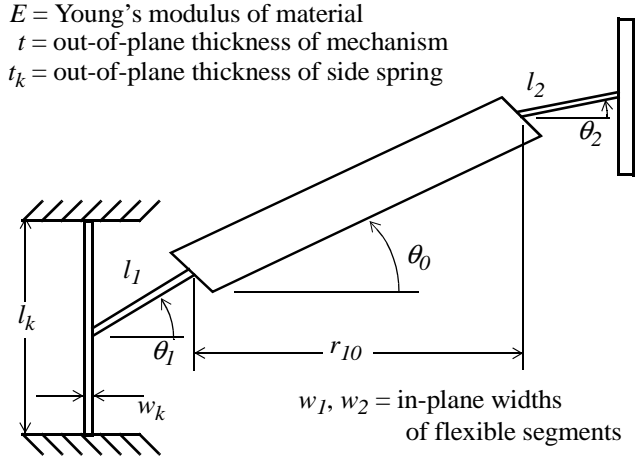


Figure 3: Parameterization for half-model used in finite element model

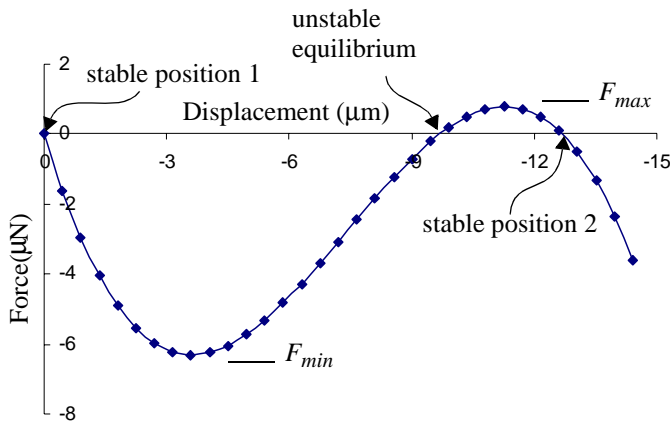


Figure 4: A force / displacement curve for a bistable mechanism.

reaching a maximum of F_{max} , before falling again to zero at the second stable position. Moreover, F_{max} is the value of the maximum force that the mechanism can exert after switching, which becomes important for valves or latches. Note that the displacement values on the graph are also negative to denote displacement in the $-y$ direction.

Optimization

In order to more easily explore the design space of this mechanism typology, optimization code was linked to the finite element model using a c-code wrapper. The optimization program was used because of its ability to quickly evaluate many designs, producing designs that are optimal with respect to some objective. Objectives that have proven useful include minimization of the mechanism footprint (to reduce space required for layout), maximization of F_{max} (to increase latching force), and minimization of the distance to the second stable position (to reduce the demand on the actuator). To ensure that the

mechanism design exhibited bistable behavior, a constraint was applied to require the value of F_{max} to exceed some limit greater than zero. For designs which are not bistable, of course, F_{max} is less than zero. This and other constraints on the optimization routine are summarized in Table 1. In this table, $F_{bistable}$ is the maximum force desired, σ_{max} is the maximum stress in the device throughout its motion, S is the ultimate strength of the material along with any safety factor desired, $F_{actuator}$ is the force output of the actuator which will switch the mechanism, $\delta_{unstable}$ is the deflection to the unstable position, and $\delta_{actuator}$ is the stroke of the actuator.

The generalized reduced gradient (GRG) method, an all-purpose gradient-based optimization algorithm, was employed for most optimization runs [23]. Because of the numerical noise inherent in a nonlinear finite element solution, this method would sometimes converge to a local minimum created by noise in the solutions. Thus, to aid in the search for a global optimum, the simulated annealing algorithm, which is not gradient-based, was also used [24].

Early optimization runs revealed that the feasible design space is actually quite narrow, with many designs exceeding either the stress constraint (if the mechanism was too stiff) or the bistability constraint (if it was not stiff enough). The optimization thus proved to be a vital part of the design process, as manually changing variables to find feasible designs would have been a lengthy and tedious process.

Using this technique, three micro-switch designs were generated for varying values of the force constraints, as outlined in Table 2. These designs are intended for use in switching

Table 1: Constraints placed on optimization

Constraint	Constraint Value	Purpose
Bistability	$F_{max} \geq F_{bistable}$	Ensure bistable behavior
Stress	$\sigma_{max} \geq S$	Prevent failure
Actuator Force	$F_{min} \geq -F_{actuator}$	Ensure actuator can cause switching
Actuator Stroke	$\delta_{unstable} \leq \delta_{actuator}$	Ensure actuator can cause switching

Table 2: Constraint values for 3 designs

	Design 1	Design 2	Design 3
$F_{bistable}$	1.0 μN	2.0 μN	1.0 μN
S	1000 MPa	1000 MPa	1000 MPa
$F_{actuator}$	7.5 μN	7.5 μN	12.5 μN
$d_{actuator}$	15.0 μm	15.0 μm	15.0 μm

applications, where small size is advantageous and little force is required for latching. Therefore, the objective used for the design of these three mechanisms was the minimization of mechanism size. The predicted performance of each mechanism design is summarized in Table 3, and the parameters describing each design are presented in Table 4. For these optimization runs, the design variables optimized were r_{I0} , θ_0 , l_1 , and θ_1 . In addition, l_2 was set equal to l_1 , and θ_2 was set equal to θ_1 . All other parameters were chosen as listed in Table 4.

FABRICATION AND TESTING

Each mechanism was designed for fabrication in Sandia's Ultra-planar Multi-level MEMS Technology V (SUMMiT V), a five-layer polysilicon surface micromachining process [25]. This technology offers five distinct layers of polysilicon, denoted Poly0, Poly1, and so on. The first layer, Poly0, is attached to the substrate for wiring and generation of ground planes, leaving

Table 3: Predicted performance of 3 designs

	Design 1	Design 2	Design 3
Layout Size	220 x 140 μN	243 x 140 μN	201 x 140 μN
F_{max}	1.0 μN	2.0 μN	1.0 μN
σ_{max}	507 MPa	532 MPa	867 MPa
F_{min}	-7.5 μN	-7.5 μN	-12.5 μN
$\delta_{unstable}$	5.8 μm	6.0 μm	6.3 μm

Table 4: Parameters describing 3 designs

Parameter	Design 1	Design 2	Design 3
r_{I0} (μm)	38.8	56.2	45.1
θ_0 (rad)	0.0635	0.0595	0.0729
l_1 (μm)	21.6	18.9	14.3
l_2 (μm)	21.6	18.9	14.3
θ_1 (rad)	0.0271	0.0250	0.0438
θ_2 (rad)	0.0271	0.0250	0.0438
w_1 (μm)	1.0	1.0	1.0
w_2 (μm)	1.0	1.0	1.0
t (μm)	2.25	2.25	2.25
l_k (μm)	40.0	40.0	40.0
w_k (μm)	2.1	2.1	2.1
t_k (μm)	7.0	7.0	7.0
E (MPa)	165	165	165

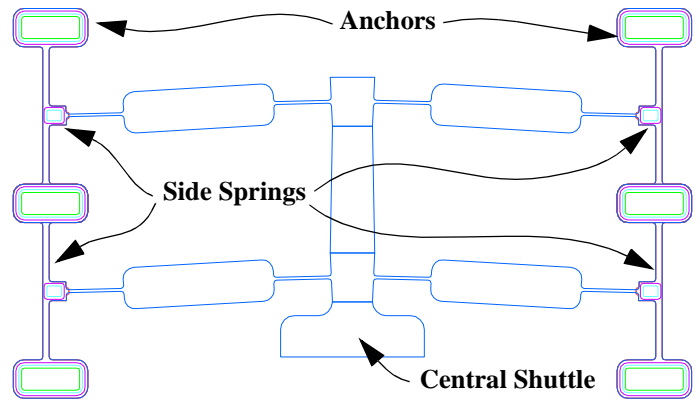


Figure 5: Layout of Design 2

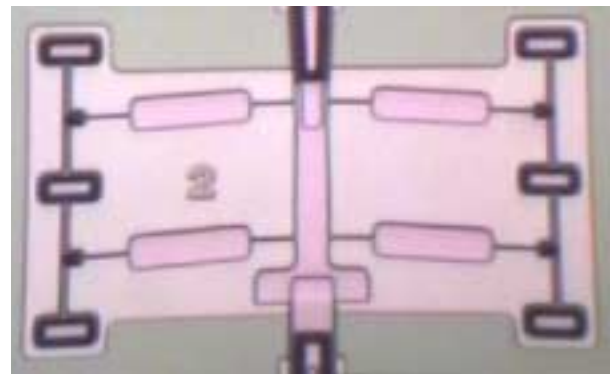
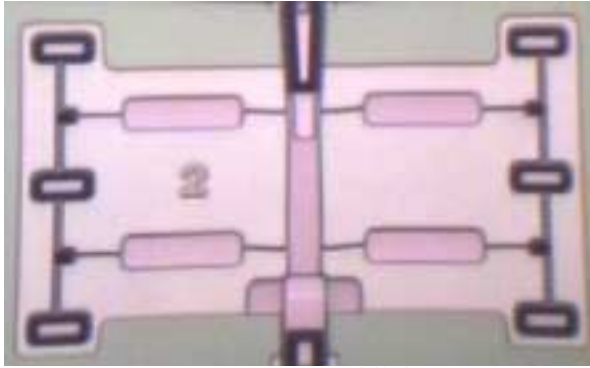


Figure 6: Photograph of Design 2, as fabricated

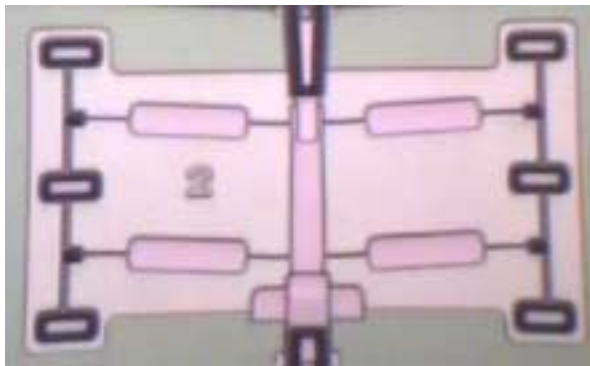
four released layers. Poly1 and Poly2 may be easily laminated, for a total combined layer thickness of 2.5 μm , while Poly3 and Poly4 are each 2.25 μm thick.

Layouts for each of the three designs were generated using the variables derived from the optimization routine. The body of each mechanism was created using Poly3 to suspend it well above the substrate, avoiding problems with stiction. The fixed-fixed beams acting as side springs were created using each of the layers, using the same dimensions in each layer. Also, the central shuttle for each mechanism was connected with the central shuttle of an identical mechanism to improve stability and prevent rotation of the device during switching. The entire device therefore consists of 4 half-models joined together in parallel. An example layout of Design 2 is shown in Fig. 5. Note that the data of Table 3 are for the device half-model, so that the predicted force values for the entire device shown in Fig. 5 are four times the values in the table.

After fabrication, the devices were released in hydrofluoric acid and then super-critically dried using a CO_2 process to prevent sticking. Fig. 6 shows a photograph of Design 2 seen through a microscope. At the bottom of the image, some optical distortion is present due to focusing problems with the camera used to capture the image. The mechanism lies between two thermal actuators (mostly out of view) for snapping in either



Near Unstable Equilibrium



Second Stable Position

Figure 7: Images of Design 2 in pre-toggle and second stable position

direction. The thermal actuators each project a small shelf of Poly4 over the bistable mechanism to prevent out-of-plane slipping between the mechanism and the actuator. These shelves are visible in the image. However, the bistable device is not physically connected to either actuator to allow snapping to occur.

Testing revealed that each mechanism snapped as expected between the two stable positions. Unfortunately, the thermal actuators did not produce as much force as expected, and they were unable to initiate bistable snapping. These actuators have been redesigned to give better performance and are currently being fabricated. However, using microprobes, each mechanism design was snapped back and forth between the two stable positions multiple times with no fracture. Fig. 7 shows Design 2 near its unstable position and in its second stable position. Both images are taken from a video (with frame rate 30 fps), in which the image near the unstable position is the last frame before the sudden snapping event. The second stable position image is the next frame after snapping.

FURTHER DESIGN SPACE EXPLORATION

The design data presented in Tables 2 and 3 demonstrate some interesting trends worth further exploration. Note that for

all three designs, the F_{max} and F_{min} constraints are both active; that is, each value is equal to its limit. This implies that smaller designs could be achieved if either constraint were relaxed somewhat. Further, Design 4, for which each of these constraints is most relaxed, is the smallest design. Thus, the data seem to indicate that smaller-sized designs are possible if the actuator force is allowed to be larger or if the maximum force near the second stable position is allowed to be smaller. As long as these two constraints are active, these two mechanism characteristics are determined by $F_{actuator}$ and $F_{bistable}$. Therefore, for designs with higher force requirements, the trend indicates that the footprint of the mechanism will have to be increased. On the other hand, $F_{actuator}$ is limited practically by the choice of actuator to be used. Thus, in the design of a bistable mechanism for minimum size, $F_{actuator}$ should be set as high as possible for the given actuator. On the other hand, a trade-off appears between minimizing size and producing necessary force near the second stable position.

Design Trade-Off Exploration

The coupled finite element analysis and optimization models were used to explore the design trade-off between the layout footprint of the mechanism and the maximum force in the second stable position, F_{max} . The value of the bistability constraint, $F_{bistable}$, is systematically varied for each optimization run. The activity of this constraint is the key to determining the relationship between layout size and F_{max} since when active, $F_{max} = F_{bistable}$. Anticipating an actuator force of approximately $50\mu\text{N}$, the value of the actuator force constraint, $F_{min} \geq -F_{actuator}$, was set to $12.5\mu\text{N}$ for the half-model. A value of $2\mu\text{N}$ was chosen as the minimum for F_{max} to ensure that it would be of significant magnitude to maintain the second equilibrium position.

The size of the resistive side-spring element was held constant at $5\mu\text{m} \times 5\mu\text{m}$ throughout the optimization, simplifying the objective function to the overall length of the mechanism (the sum of the lengths of the small-length flexural pivots and the stiff member between them). The small size of this extremely stiff spring requires little layout space and facilitates the minimization of the length of the other typology members.

The results from this study are shown in Fig. 8. The length of the mechanism is given in μm and the force in μN . Both the actuator force and bistability force constraints were active for all designs. As the preliminary data implied, the finite element analysis indicates that the minimum layout size increases with the maximum force in the second stable position. From a design perspective, this means that for this topology, a mechanism capable of producing a certain latching force requires a minimum layout size. As the latching force needs increase, the layout space allocated to the mechanism must also increase. The arrows to the right of the solid line indicate “feasible space.” Viable mechanisms can be created for any $(F_{max}, length)$ pair in that space.

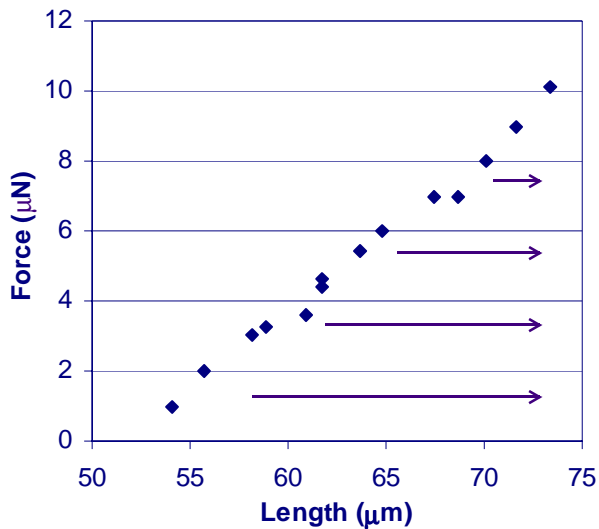


Figure 8: Results from layout size and force in the second stable position design exploration. Viable mechanisms can be created for any point to the right of the line.

CONCLUSION

Fully-compliant bistable micromechanisms were modeled using finite elements. By linking the finite element model to an optimization program, the design space was extensively explored. Three designs within this space were generated by minimizing the layout size of the devices subject to force constraints. These designs were subsequently manufactured and tested to ensure bistable behavior. Testing revealed that each mechanism snapped as expected between the two stable positions.

The design space was then further explored to determine the behavior of the device as the maximum force output increased. This study revealed that the minimum layout size increases with the maximum force output. From a design perspective, this means that for the given mechanism topology, a device capable of producing a certain latching force requires a minimum layout size. For an increase in the required latching force, the necessary layout space must also increase.

ACKNOWLEDGEMENTS

Thanks is given to the University of Michigan Computer Aided Engineering Network for use of the computing facilities. The fabrication work of the staff of the Microelectronics Development Laboratory at Sandia National Laboratories is also gratefully acknowledged. This work is supported under a National Science Foundation Graduate Research Fellowship and a National Science Foundation CAREER Award. Sandia is a

multiprogram laboratory operated by Sandia Corporation, a Lockheed Martin Company, for the United States Department of Energy under contract DE-AC04-94AL85000.

REFERENCES

- [1] B. Wagner, H.J. Quenzer, S. Hoershelmann, T. Lisec, M. Juerss, Bistable Microvalve with Pneumatically Coupled Membranes, *Proc. IEEE Micro Electro Mechanical Systems 1996*, 384-388.
- [2] C. Goll, W. Bacher, B. Buestgens, D. Maas, W. Menz, W.K. Schomburg, Microvalves with Bistable Buckled Polymer Diaphragms, *J. Micromech. and Microeng.*, **6** (1) (1996) 77-79.
- [3] Y. Shinozawa, T. Abe, T. Kondo, Proportional Microvalve Using a Bi-Stable Magnetic Actuator, *Proc. 1997 IEEE Micro Electro Mechanical Systems (MEMS)*, 233-237.
- [4] W.K. Schomburg, C. Goll, Design Optimization of Bistable Microdiaphragm Valves, *Sens. & Act., A: Phys.*, **64** (3) (1998) 259-264.
- [5] B. Hälg, On A Nonvolatile Memory Cell Based on Micro-electro-mechanics, *IEEE Micro Electro Mechanical Systems 1990*, 172-176.
- [6] H. Matoba, T. Ishikawa, C. Kim, R.S. Muller, A Bistable Snapping Mechanism, *IEEE Micro Electro Mechanical Systems 1994*, 45-50.
- [7] E.J.J. Kruglick, K.S.J. Pister, Bistable MEMS Relays and Contact Characterization, *1998 Solid-State Sensor and Actuator Workshop*, 333-337.
- [8] X. Sun, K.R. Farmer, W. Carr, Bistable Microrelay Based on Two-Segment Multimorph Cantilever Actuators, *Proc. 1998 IEEE Micro Electro Mechanical Systems (MEMS)*, 154-159.
- [9] M. Vangbo, Y. Bäccklund, A Laterally Symmetrically Bistable Buckled Beam, *J. Micromech. & Microeng.*, **8** (1998) 29-32.
- [10] B.D. Jensen, L.L. Howell, L.G. Salmon, Design of Two-Link, In-Plane, Bistable Compliant Micro-Mechanisms, *J. Mech. Des.*, **121** (3) (1999) 416-423.
- [11] J. Qiu, J.H. Lang, A.H. Slocum, A Centrally-Clamped Parallel-Beam Bistable MEMS Mechanism, *Proc. IEEE Micro Electro Mechanical Systems (MEMS) 2001*, CH37090, 353-356.
- [12] M. Hoffman, P. Kopka, T. Gross, E. Voges, Optical Fibre Switches Based on Full Wafer Silicon Micromachining, *J. Micromech. & Microeng.*, **9** (2) (1999) 151-155.
- [13] F. Pieri, M. Piotta, A Micromachined Bistable 1X2 Switch for Optical Fibers, *Microelectronic Eng.*, **53** (1) (2000) 561-564.
- [14] H. Maekoba, P. Helin, G. Reyne, T. Bourouina, H. Fujita, Self-Aligned Vertical Mirror and V-grooves Applied to an Optical-Switch: Modeling and Optimization of Bi-Stable Operation by Electromagnetic Actuation, *Sensors and Actuators, A: Physical*, **87** (3) (2001) 172-178.

- [15] J.G. Fleming, Bistable membrane approach to micromachined displays, *Flat Panel Display Materials - 1998 MRS Symposium*, Vol. 508, 219-224.
- [16] M.T.A. Saif, On a Tunable Bistable MEMS—Theory and Experiment, *J. MEMS*, **9** (2) (2000) 157-169.
- [17] W. Fang, J.A. Wickert, Comments on Measuring Thin-Film Stresses Using Bi-layer Micromachined Beams, *J. Micromechanics & Microengineering*, **5** (1995) 276-281.
- [18] V. Ziebart, O. Paul, U. Münch, S. Jürg, H. Baltes, Mechanical Properties of Thin Films from the Load Deflection of Long Clamped Plates, *J. MEMS*, **7** (3) (1998) 320-328.
- [19] M.B. Parkinson, B.D. Jensen, G.M. Roach, Optimization-Based Design of a Fully-Compliant Bistable Micromechanism, *Proc. ASME Design Engineering Technical Conferences 2000*, DETC2000/MECH-14119.
- [20] G.K. Ananthasuresh, S. Kota, The Role of Compliance in the Design of MEMS, *Proc. 1996 ASME Design Engineering Technical Conferences*, 96-DETC/MECH-1309.
- [21] L.L. Howell, *Compliant Mechanisms*, John Wiley and Sons, New York, NY, 2001.
- [22] L.L. Howell, A. Midha, A Method for the Design of Compliant Mechanisms with Small-Length Flexural Pivots, *ASME Journal of Mechanical Design*, **116** (1) (1994) 280-290.
- [23] A.R. Parkinson, M. Wilson, Development of Hybrid GRG-SQP Algorithm for Constrained Nonlinear Programming, *J. of Mech. Trans. and Automation in Design*, Trans. ASME, **110** (1988) 308.
- [24] S. Kirkpatrick, C.D. Gelatt, M.P. Vecchi, Optimization by Simulated Annealing, *Science*, **22** (459) (1983) 671.
- [25] <http://www.mems.sandia.gov>